iScience

CellPress
OPEN ACCESS

Article

Calcium carbonate mineralization is essential for biofilm formation and lung colonization

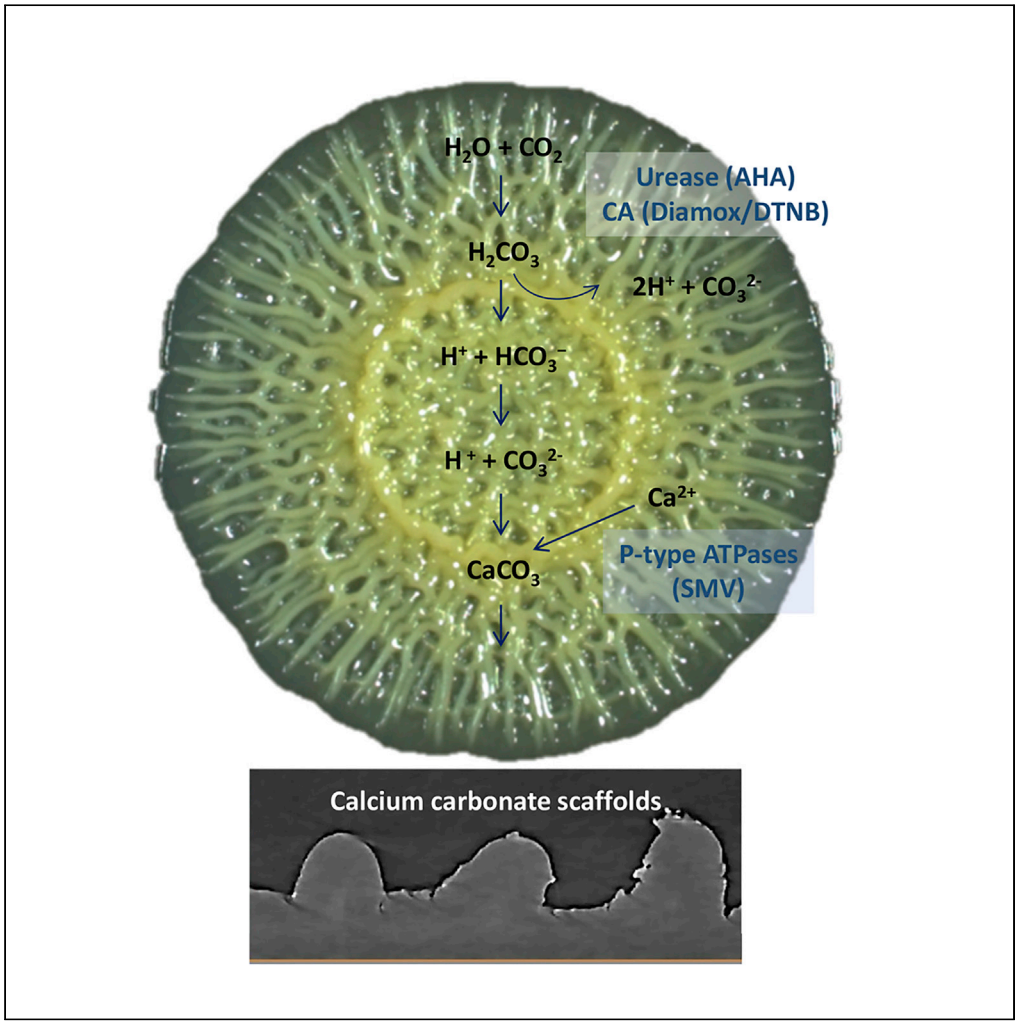

Malena Cohen-Cymberknoh, Dror Kolodkin-Gal, Alona Keren-Paz, ..., Gideon Zamir, Eitan Kerem, Ilana Kolodkin-Gal

eitank@hadassah.org.il (E.K.)
ilana.kolodkin@mail.huji.ac.il (I.K.-G.)

Highlights

3D microCT X-ray reveals mineral scaffolds in *Pseudomonas aeruginosa*

Calcium carbonate production promotes the formation of *Mycobacterium abscessus* biofilms

Calcium carbonate production is associated with lung colonization by *P. aeruginosa*

Targeting biomineralization reduced the damage inflicted by biofilms to the lung

Cohen-Cymberknoh et al., iScience *25*, 104234
May 20, 2022
https://doi.org/10.1016/j.isci.2022.104234

iScience

CellPress
OPEN ACCESS

Article

Calcium carbonate mineralization is essential for biofilm formation and lung colonization

Malena Cohen-Cymberknoh,[1,9] Dror Kolodkin-Gal,[2,9] Alona Keren-Paz,[3,4,9] Shani Peretz,[3] Vlad Brumfeld,[5] Sergey Kapishnikov,[5] Ronit Suissa,[3] Michal Shteinberg,[6] Daniel McLeod,[7] Harsh Maan,[3] Marianna Patrauchan,[7] Gideon Zamir,[2] Eitan Kerem,[1,*] and Ilana Kolodkin-Gal[3,8,10,*]

ABSTRACT

Biofilms are differentiated microbial communities held together by an extracellular matrix. μCT X-ray revealed structured mineralized areas within biofilms of lung pathogens belonging to two distant phyla – the proteobacteria *Pseudomonas aeruginosa* and the actinobacteria *Mycobacterium abscessus*. Furthermore, calcium chelation inhibited the assembly of complex bacterial structures for both organisms with little to no effect on cell growth. The molecular mechanisms promoting calcite scaffold formation were surprisingly conserved between the two pathogens as biofilm development was similarly impaired by genetic and biochemical inhibition of calcium uptake and carbonate accumulation. Moreover, chemical inhibition and mutations targeting mineralization significantly reduced the attachment of *P. aeruginosa* to the lung, as well as the subsequent damage inflicted by biofilms to lung tissues, and restored their sensitivity to antibiotics.

This work offers underexplored druggable targets for antibiotics to combat otherwise untreatable biofilm infections.

INTRODUCTION

In nature, bacteria form complex and differentiated multicellular communities known as **biofilms**. The coordinated actions of many cells communicating and dividing labor improve the ability of the community to attach to hosts and protect it from environmental assaults (Aguilar et al., 2007; Harris and Kolodkin-Gal, 2018). Microbial biofilms are of extreme clinical importance because they are associated with many persistent and chronic infections (Costerton et al., 1999). For example, the commensal/aquatic bacterium *Pseudomonas aeruginosa* can cause devastating chronic biofilm infections in compromised hosts, such as cystic fibrosis (CF) patients and those with burn wounds or implanted medical devices (Costerton et al., 1999). Respiratory infections with *P. aeruginosa* are a leading cause of morbidity and mortality in patients with CF (Yoon and Hassett, 2004). Once a chronic infection with *P. aeruginosa* is established, it is almost impossible to eradicate (Cohen-Cymberknoh et al., 2016). Similarly, the biofilms of *Mycobacterium abscessus* cause infections of the respiratory tract, skin, and central nervous system in patients with CF and chronic obstructive pulmonary disease (Caimmi et al., 2018).

A prominent feature of biofilms is their inherent resistance to the immune system and antibiotics (Bryers, 2008; Bucher et al., 2019; Hill et al., 2005) – biofilm cells are up to 1,000 times more tolerant than planktonic bacteria (Bryers, 2008), making the eradication of biofilm infections with currently available antibiotics extremely challenging. In a biofilm, self-produced polymers constitute the extracellular matrix (ECM), which binds bacterial cells to each other and the surface. The ECM plays an important role in the resistance and resilience of the entire biofilm community. To date, the ability of biofilm-forming bacteria to generate complex architectures was exclusively attributed to their **organic** ECM (Rani et al., 2007; Stewart and Franklin, 2008; Xu et al., 1998). The most extensively studied components of biofilm organic ECMs are carbohydrate-rich polymers (i.e., extracellular polysaccharides or exopolysaccharides) (Branda et al., 2005). Various genetic analyses have provided strong evidence that biofilm exopolysaccharides play a fundamental structural role in biofilms of different bacterial species. For example, *P. aeruginosa* isolates from lungs of cystic fibrosis (CF) patients were shown to overproduce alginate, resulting in a mucoid colony phenotype. Another two exopolysaccharides, Pel and Psl, play redundant roles in defining the ECM

[1]Pediatric Pulmonary Unit and Cystic fibrosis Center, Hadassah Medical Center and Faculty of Medicine, Hebrew University of Jerusalem, Israel

[2]Department of Experimental Surgery, Hadassah-Hebrew University Medical Center, Jerusalem, Israel

[3]Department of Molecular Genetics, Weizmann Institute of Science, Rehovot, Israel

[4]National Center for Antibiotic Resistance and Infection Control, Tel Aviv Medical Center, Tel Aviv, Israel

[5]Chemical Research Support, Weizmann Institute of Science, Rehovot, Israel

[6]Pulmonology Institute and CF Center, Carmel Medical Center, Haifa, Israel

[7]Department of Microbiology and Molecular Genetics, Oklahoma State University, Stillwater, OK, USA

[8]Present address: Department of Plant Pathology and Microbiology, Faculty of Agriculture, Food and Environment, The Hebrew University of Jerusalem, Rehovot, Israel

[9]These authors contributed equally

[10]Lead contact

*Correspondence: eitank@hadassah.org.il (E.K.), ilana.kolodkin@mail.huji.ac.il (I.K.-G.)

https://doi.org/10.1016/j.isci.2022.104234

structure of *P. aeruginosa* (Colvin et al., 2012). Biofilm colonies are a compelling model system for biofilm development, and many essential biological processes of high relevance to bacterial pathogenicity were first discovered in this well-controlled and robust system (Colvin et al., 2012; Dietrich et al., 2008; El Mammeri et al., 2019; Hufnagel et al., 2018; Jo et al., 2017; Richards et al., 2019; Serra et al., 2013; Steinberg et al., 2020; Wermser and Lopez, 2018).

In addition to organic exopolymers, recent studies highlighted the role for self-produced minerals in biofilm development. In 1998, it was determined that biofilms of *Proteus mirabilis, Proteus vulgaris, and Providencia rettgeri* caused extensive catheter encrustation by calcium and magnesium minerals within 24 h (Stickler et al., 1998). Additional evidence for minerals being an intrinsic feature of the biofilm lifestyle emerged in 2015 in the Gram-negative pathogen *P. aeruginosa* (Li et al., 2015). By using real-time confocal laser reflection and calcein staining *in vitro*, they observed growing minerals within a biofilm dominated by calcium carbonate (as judged by Raman spectroscopy). Furthermore, carbonic anhydrase was shown to mediate calcium deposition in *P. aeruginosa* biofilms (Lotlikar et al., 2019). Most recently, calcium cations were found to cross-link negatively charged alginate polymers (Jacobs et al., 2022).

In parallel, our group demonstrated that a urease mutant fails to properly assemble *Bacillus subtilis* biofilms. We hypothesized that the controlled deposition of a calcium carbonate scaffold could structurally support the morphogenesis of bacterial colonies (Keren-Paz et al., 2018; Oppenheimer-Shaanan et al., 2016).

Although organic matrices and their regulation differ between microorganisms (Steinberg and Kolodkin-Gal, 2015), the formation of calcium carbonate relies on simple building blocks, calcium, and carbonate, generated from carbon dioxide in most heterotopic organisms. Therefore, the generation of mineral scaffolds could be common and conserved across the bacterial domain, contributing to the phenotypical resistance of diverse microbial biofilms. If so, understanding the underlying molecular mechanisms of biofilm mineralization is a crucial step toward our ability to successfully combat biofilm infections.

In this work, we discovered that the calcium-dependent 3D organization of the biofilm colony leads to transcriptional reprogramming of the bacterial community and was essential for biofilm development. Calcium carbonate was produced by two unrelated lung pathogens – *P. aeruginosa* and *M. abscessus*. Inhibition of key biomineralization enzymes or calcium uptake prevented biofilm formation by both pathogens. We were able to identify calcite in sputum samples taken from CF patients, suggesting that this conserved process is of clinical importance. Finally, in an *ex vivo* lung model, chemical and genetic inhibition of calcium uptake and carbonate accumulation blocked biofilm formation and lung colonization, preventing damage inflicted by *P. aeruginosa* to lung tissues, and sensitized *P. aeruginosa* to antibiotic treatment.

Taken together, our results identify a previously overlooked process essential for bacterial biofilm development – **the biologically regulated formation of mineral scaffolds**. Its conservation across the bacterial kingdom highlights the fundamental role of biomineralization in biofilm biology and could lead to new therapeutic approaches for combating a broad range of persistent biofilm infections.

RESULTS

3D microCT X-ray reveals calcium scaffolds in *P. aeruginosa* colonies

We have recently reported that, like *B. subtilis*, the biofilm colonies of soil actinobacterium *Mycobacterium smegmatis* contain functional mineral macro-structures (Oppenheimer-Shaanan et al., 2016). One additional study provided evidence for some spatial organization of calcium carbonate minerals in submerged biofilms formed by the Gram-negative pathogen *P. aeruginosa* (Li et al., 2016a). This led us to explore whether we can detect the regulated formation of functional mineral structures in pathogenic biofilm colonies. We hypothesized that mineral formation might be a common phenomenon in the bacterial kingdom (Keren-Paz et al., 2018; Keren-Paz and Kolodkin-Gal, 2020; Li et al., 2015,2016a; Oppenheimer-Shaanan et al., 2016).

When grown on biofilm-inducing agar *P. aeruginosa* PA14 forms complex colonies with a highly characteristic morphology which were shown to be dependent on polysaccharides encoded by the *pel* operon (Colvin et al., 2011). However, these complex 3D structures were co-localized with spatially organized minerals, as determined by microCT (Figure 1A), were abolished by the cation chelator EDTA and EGTA, and could

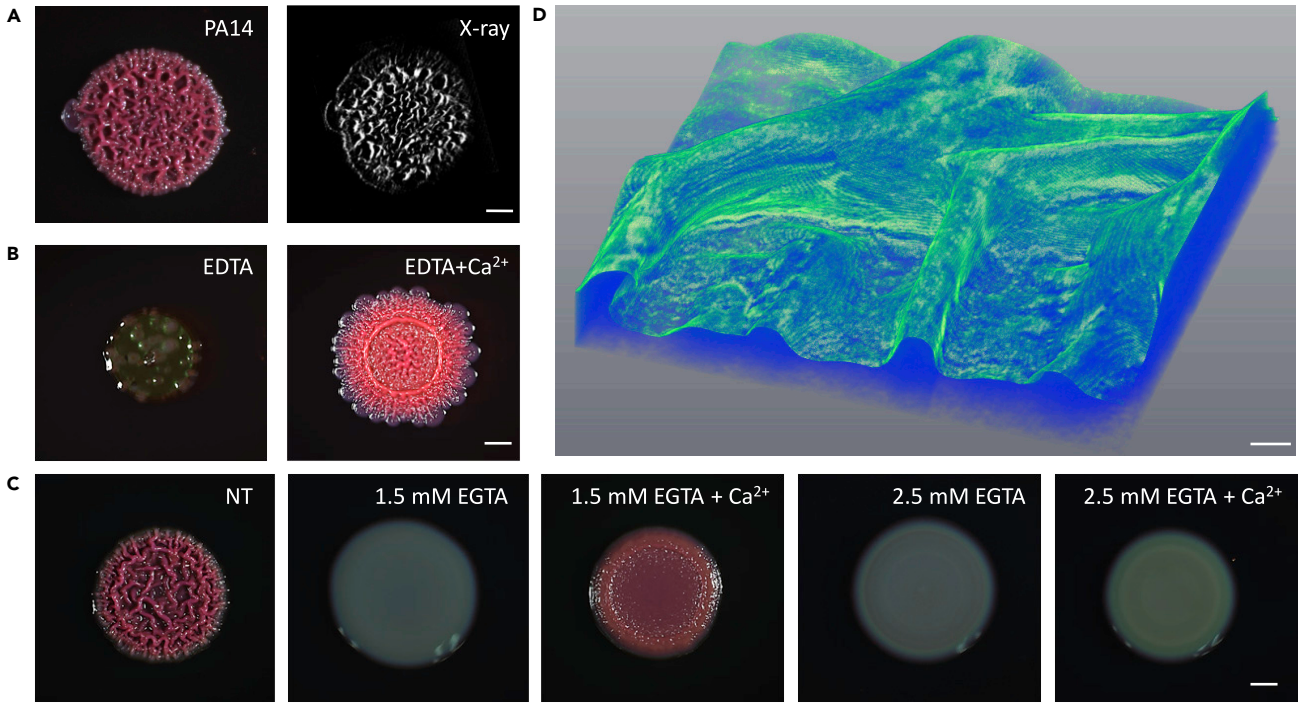

Figure 1. The role of calcium in the biofilm structure is conserved across bacterial species

(A) Light microscopy (left) and microCT-X-ray (right) images of 3-day-old *P. aeruginosa* PA14 biofilm colonies grown on TB agar. In the X-ray images, the bright contrast appears white, and indicates the location of dense mineral whereas the organic matter appears dark. Scale bar – 1 mm. A representative image (out of n = 3 experiments) is shown.

(B) Light microscopy images of 3-day-old *P. aeruginosa* PA14 of biofilm colonies grown on TB agar supplemented with 1 mg/mL EDTA (chelating agent), either with or without the addition of 700 mM $CaCl_2$. Scale bar – 1 mm. A representative experiment (out of n = 3 experiments) is shown.

(C) Light microscopy images of 3-day-old *P. aeruginosa* PA14 biofilm colonies, grown on TB agar either untreated (NT), or supplemented with 700 mM $CaCl_2$ and EGTA (calcium chelator), as indicated. Scale bar – 5 mm. A representative image (out of n = 3 experiments) is shown.

(D) 3D reconstruction of microCT X-ray analysis revealing mineral distribution in a 5-dayold *P. aeruginosa* PA14 colony. The color indicates intensity, with green representing the densest mineral. Scale bar – 0.2 mm. A representative image (out of n = 3 experiments) is shown.

be restored by the addition of excess calcium (Figures 1B and1C). To create the 3D reconstruction, a whole, unfixed bacterial colony was transferred to a plastic slide for a microCT scan and rotated between the X-ray source and the detector positioned at optimal distances for a voxel size of 0.87 μm. 2D projections were taken at different angles until a full rotation (360°) was completed. The full set of images was then used to reconstruct the whole volume of the sample by back- projection algorithm, and thus a high-resolution 3D image was generated (see Videos S1 and S2). This microCT X-ray scan confirmed that the crystalline calcium scaffold on *P. aeruginosa* is organized in a macro-structure and that the densest mineral areas formed a non-continuous layer correlated with colony wrinkles (Figure 1D), further suggesting that the 3D structure of *P. aeruginosa* biofilms likely relies on the formation of calcite mineral scaffolds. Consistently, the calcein stain indicated the accumulation of calcium (which preferentially stains extracellular calcium because of its poor permeability through membranes) within the biofilms (Figure S1). The formation of elaborate calcium-dependent 3D morphology was conserved in an additional strain of *P. aeruginosa* PA01 (Figure S2). The effect of chelating calcium cations under our conditions was specific, as neither magnesium nor iron restored the 3D morphology (Figure S2).

The production of calcium carbonate is associated with complex structure and biofilm formation of *P. aeruginosa*

The cellular pathways of biomineralization present in bacteria are well conserved (Figure 2A) and can be inhibited at several points. The role of urease and carbonic anhydrase (CA) in biomineralization is well established (Jansson and Northen, 2010; Phoenix and Konhauser, 2008). In *P. aeruginosa*, urea is a natural product of arginine fermentation (Park et al., 1997). The precipitation of carbonates via urea hydrolysis is a straightforward mechanism to produce high amounts of carbonates in a short period of time (1 mol of

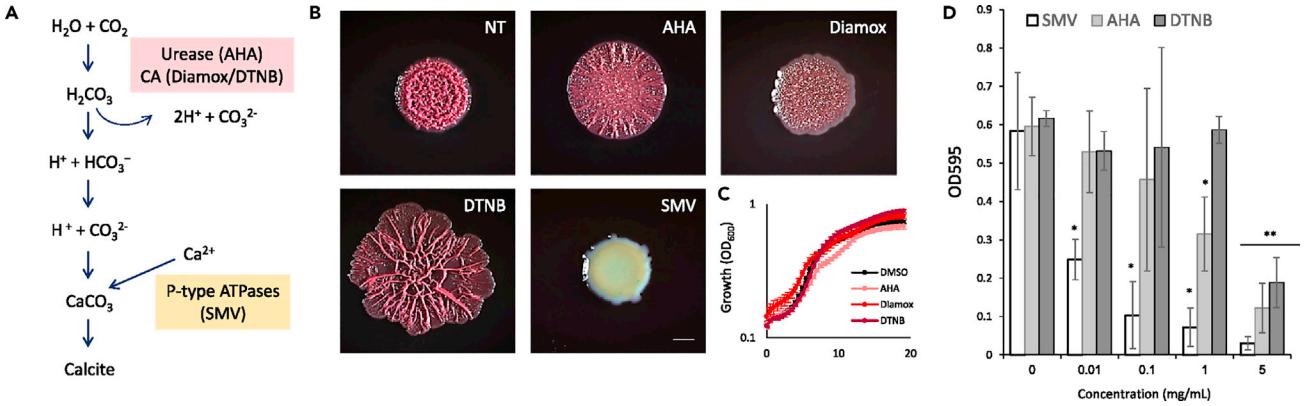

Figure 2. Inhibition of cellular pathways leading to calcium carbonate production disrupts biofilm development in *P. aeruginosa*.

(A) A schematic representation of the chemical reaction leading to calcium carbonate production, with the inhibitors used in this study indicated in parentheses next to the step they inhibit.

(B) Light microscopy images of 3-day-old *P. aeruginosa* PA14 biofilm colonies grown on TB agar containing the inhibitors indicated in (A) as follows: untreated (NT), 1.5 mg/mL DTNB, 1.75 mg/mL AHA, 2.5 mg/mL Diamox and 0.01 mg/mL SMV. Scale bar – 2 mm. A representative image (out of n = 3 experiments) is shown.

(C) The effect of inhibiting calcium carbonate production on planktonic growth of *P. aeruginosa* PA14. Bacteria were grown shaking in liquid TB medium, supplemented with: 1.5 mg/mL DTNB, 1.75 mg/mL AHA, 2.5 mg/mL Diamox and 0.01, 0.05 and 0.01 mg/mL SMV, or untreated (NT). Growth was monitored by measuring OD600 in a microplate reader every 30 min. Results are averages of six wells, bars represent standard deviations. A representative experiment (out of n = 3 experiments) is shown.

(D) Crystal violet assay quantifying biofilm formation of *P. aeruginosa* PA14, grown in BHI supplemented with the indicated inhibitors. Results are averages and standard deviation of three independent experiments. P values, as determined by Student's *t*-test are indicated (* pVal <0.01, ** pVal <0.001, when compared to the untreated control).

urea is hydrolyzed to 1 mol of ammonia and 1 mol of carbonate, which spontaneously hydrolyzes to form an additional 1 mol of ammonia and carbonic acid). Thus, CAs and urease independently contribute to carbonate production and calcium carbonate mineralization.

Consistent with the central role of calcium carbonate scaffolds in supporting biofilm morphology, the inhibition of urease by AHA (Li et al., 2020), CA by Diamox (Supuran, 2011), and P-type ATPases by vanadate salt (Guragain et al., 2013), disrupted *P. aeruginosa* biofilm morphology (Figure 2B). These interventions abolished the mineral macrostructures as judged by microCT X-ray (Figure S3). This effect could not be explained by the inhibition of planktonic growth, which was mostly unaffected (Figures 2C and S4). Biofilm formation on polystyrene, as quantified by crystal violet staining, was also severely compromised by either chemically impairing carbonate formation or calcium homeostasis (Figure 2D). Similarly, depleting atmospheric carbon dioxide and aerobic respiration (where carbon dioxide is the main byproduct) reduced the mineral macrostructure (Figure S5).

Chemical inhibition of enzymes can also exert an off-target effect. Hence, we tested clean mutants in the mentioned biomineralization pathways. Inhibition of complex calcium-dependent colony formation, but not planktonic growth, was also observed in mutants lacking two or more carbonic anhydrase genes (Lotlikar et al., 2019) or a calcium transporter CalC (Figure 3A). The fact that SMV addition or CalC deletion could prevent 3D morphology development and biofilm formation, but had little effect on planktonic growth (Figure 3B), is consistent with our view that carbonate mineralization in biofilms relies on the regulation of intracellular calcium homeostasis and biofilm formation on polystyrene (Figure 3C). The inhibition on polystyrene surfaces (in contrast with biofilm colonies) was time-dependent (Figure S6), demonstrating that the dependence of structured colony formation on these processes is higher than that of the submerged biofilm. The mineral and exopolysaccharides were essential for structure formation, as a mutant for both pel and psl operons was flat and featureless, similarly to biofilms grown with a calcium chelator (Figure 3D). In addition, the operons were essential for submerged biofilm formation on polystyrene plates (Figure S7). The formation of an organic carbohydrates-based matrix (Friedman and Kolter, 2004) was not necessary for extracellular calcium accumulation as judged by calcein stain that is not membrane permeable, although the intensity of the stain was reduced (Figure S8).

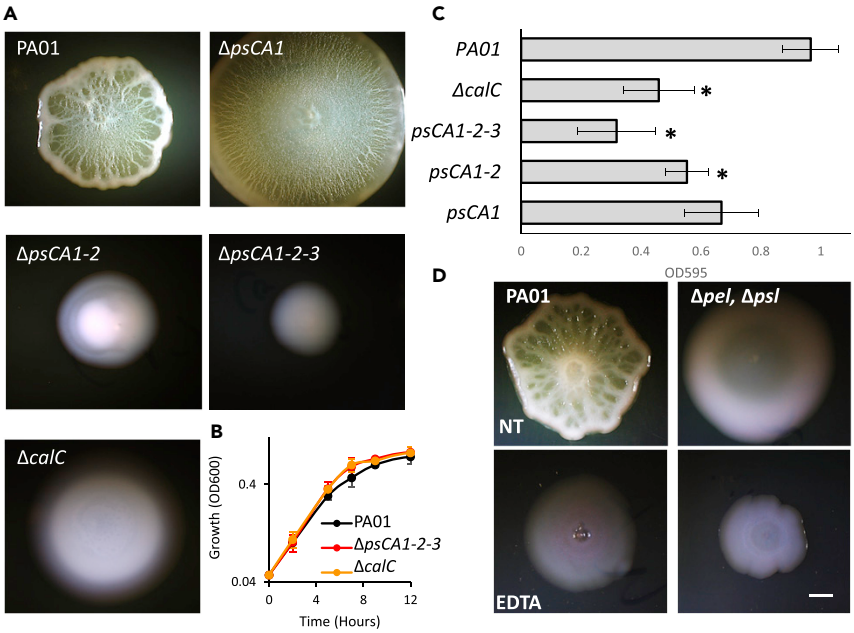

Figure 3. Biofilm development is compromised in *P. aeruginosa* mutants for cellular pathways of calcium carbonate production

(A) Light microscopy images of 4-day-old biofilm colonies of wild type *P. aeruginosa PA01* and indicated mutants grown on BHI agar: carbonic anhydrases (*psCA1*– PA0102, *psCA2* - PA2053, *psCA3*– PA4676) and calcium channel (Δ*calC*). A representative experiment (out of n = 3 experiments) is shown. Insert – the indicated mutant strains were grown planktonically in shaking liquid BHI medium.

(B) Growth was monitored by measuring OD600 in a spectrophotometer at indicated times. Results are averages of four wells, bars represent standard deviations. Scale bar – 2 mm. A representative experiment (out of n = 3 experiments) is shown.

(C) Crystal violet assay quantifying biofilm formation of wild type and indicated mutant derivates of *P. aeruginosa* PA01, grown with in liquid BHI medium for 10 h. Results are averages and standard deviation of three independent experiments. p values, as determined by Student's *t*-test are indicated (* pVal <0.01, when compared to the untreated control).

(D) Light microscopy of biofilm colonies of *P. aeruginosa* PA01 either untreated or supplemented with EDTA (0.1 mg/mL) as indicated. Colonies were grown on BHI solid medium for 4 days at 23°C. Scale bar = 5 mm. The experiment was repeated 2 times, in a technical three repeats – and representative images are shown.

The production of calcium carbonate is associated with complex structure and biofilm formation of *M. abscessus*

To indicate whether the formation of mineral scaffolds is a conserved process of significant clinical potential, we tested whether it occurs in another, phylogenetically distant, drug-resistant pathogen. We, therefore, examined the biofilms of *M. abscessus*, which are held together by an extracellular matrix consisting of mycolic acids (Halloum et al., 2016), which bear little resemblance to EPS components of *P. aeruginosa*. Nevertheless, this bacterium also only formed colonies of complex morphology in the presence of calcium (Figures 4A and 4B) on B4 biofilm and mineralization medium (Barabesi et al., 2007).

Fourier transform infrared spectroscopy (FTIR) was used to confirm calcium carbonate (in this method, carbonate minerals can be distinguished as ν_4 peak is expected at 713 cm^{-1} for calcite, 750 cm^{-1} for vaterite and 715 cm^{-1} for aragonite (Politi et al., 2004). Indeed crystalline calcium carbonate mineral was detected in the colony (Figure S9). X-ray analysis revealed that the densest mineral areas were co-localized with colony wrinkles (Figure 4C; Videos S3 and S4), just like in *P. aeruginosa* colonies. In addition to the organized macro-scale structures present throughout the colony, ; large crystals also formed beneath the colony and in its periphery over time. In both *P. aeruginosa* and *M. abscessus* colonies, mineral macrostructures form in a slightly basic-neutral macro pH (Figure S10). Under such conditions, passive mineral precipitation is unlikely, supporting a potential biological regulation of mineralization.

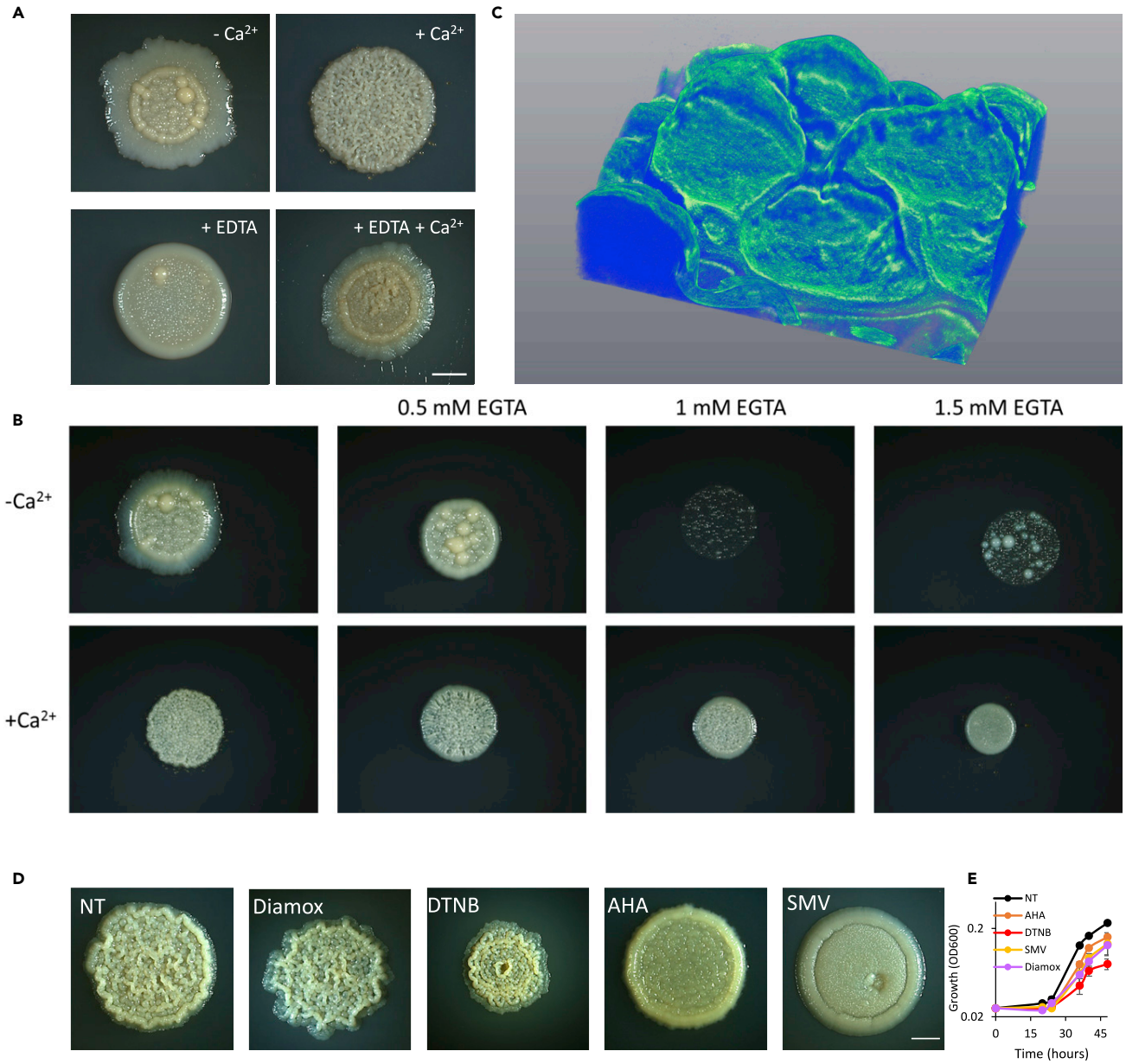

Figure 4. Inhibition of cellular pathways leading to calcium carbonate production disrupts biofilm development in *M. abscessus*

(A) Light microscopy images of 5-day-old *M. abscessus* biofilm colonies, grown on B4 agar, supplemented with either calcium acetate (0.25% v/v), or 1.5 mM EDTA, as indicated. Scale bar – 5 mm. A representative image (out of n = 3 experiments) is shown.

(B) Light microscopy images of 3-day-old *M. abscessus* biofilm colonies grown on B4 agar, either untreated (NT) or supplemented with 700 mM $CaCl_2$ and EGTA, as indicated. Scale bar – 5 mm. A representative experiment (out of n = 3) experiments is shown.

(C) 3D rreconstructionof microCT X-ray analysis revealing mineral distribution in a 5-dayold *M. abscessus* colony grown on B4 agar with calcium. Color indicates intensity, with green representing the densest mineral. Scale bar – 0.1 mm. A representative image (out of n = 3 experiments) is shown.

(D) Light microscopy images of 5-day-old *M. abscessus* biofilm colonies, grown on B4 agar supplemented with calcium and 2.5 mM of the indicated inhibitors or untreated (NT). A representative experiment (out of n = 3) experiments is shown. (E) *M. abscessus* was grown planktonically in a liquid B4 medium. Growth was monitored by measuring OD_{600} in a spectrophotometer at indicated times. Scale bar – 2 mm. Results are averages of three independent repeats, bars represent standard deviations.

The potentially broad clinical implication of these findings was supported by testing chemical inhibitors on *M. abscessus*. Colony morphology could be compromised by inhibiting biomineralization enzymes (Figures 4D and S11). Morphology defects could not be explained by cell growth inhibition because

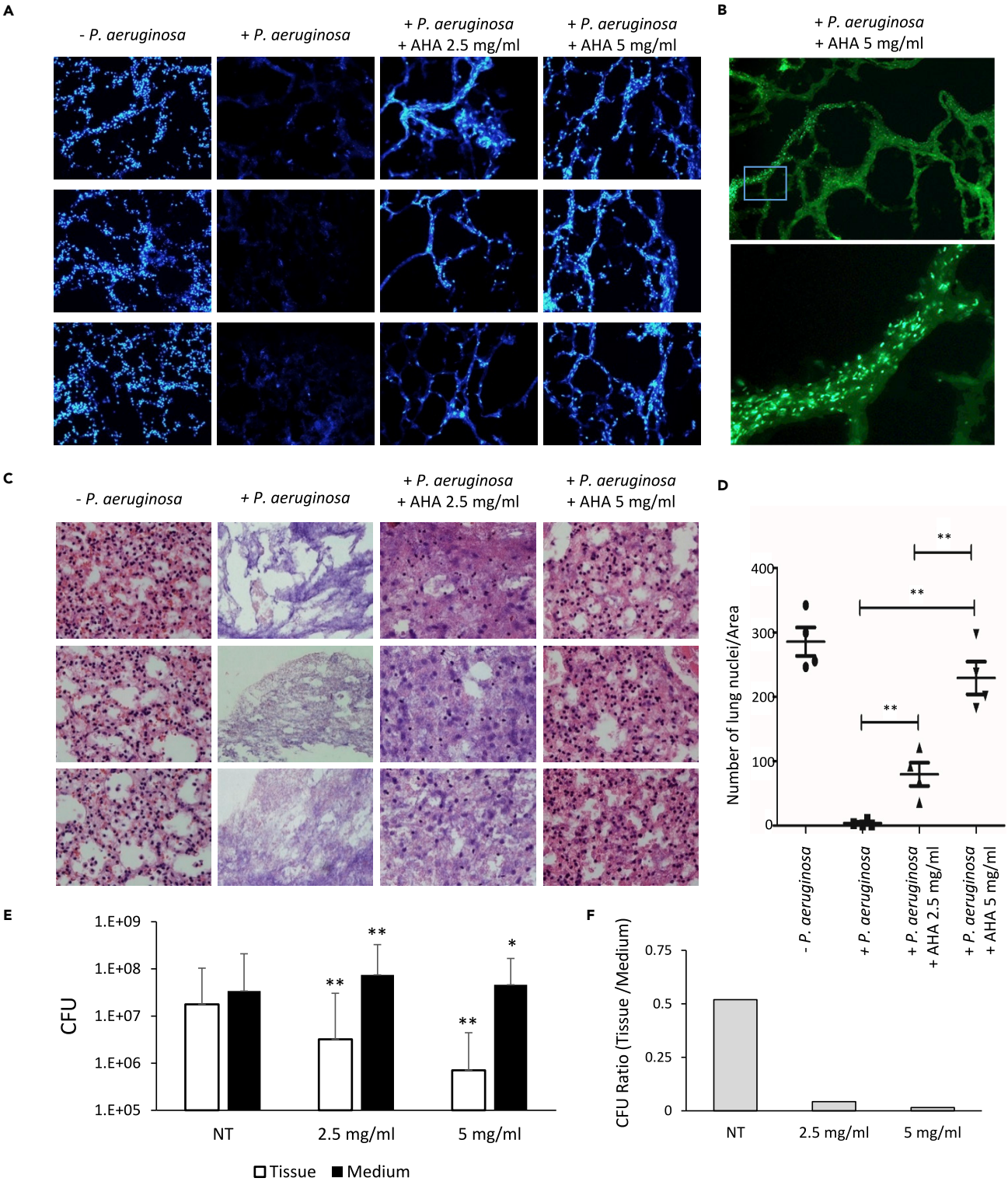

Figure 5. Urease inhibition prevents biofilm formation and tissue deterioration in an *ex-vivo* lung model.

(A and B) Fluorescent microscopy images of 10 micron slices of lung tissues, infected with *P. aeruginosa* PA14 and treated with AHA, as indicated. (A) Blue – lung cell nuclei stained by DAPI, (magnification ×20). (B) Green - GFP expressing *P. aeruginosa*, (magnification ×40). A representative experiment (out of n = 3) experiments is shown.

Figure 5. *Continued*

(C) Light microscopy images of 7 micron slices of lung tissue. Samples were treated as in (A), and stained with hematoxylin and eosin (H&E). Blue – nuclei, red – extracellular matrix and cytoplasm, (magnification ×40). A representative experiment (out of n = 3) experiments is shown.

(D) Quantification of lung viability. Lung tissue cultures were infected with *P. aeruginosa* PA14 and treated with AHA, as indicated. ImageJ 1.51g software was used to automatically count lung cell nuclei in four randomly chosen fields for each treatment. p values, as determined by Student's *t*-test are indicated (** pVal <0.001).

(E) CFU analysis of *P. aeruginosa* PA14 infecting lung tissue and surrounding media, with and without treatment. p values, as determined by Student's *t*-test are indicated (* pVal <0.01, ** pVal <0.001, when compared to the untreated control).

(F) Quantification representing the ratios of tissue to medium CFU in (E).

most potent morphology inhibitors AHA and SMV, had the slightest effect on planktonic growth (Figure 4E). Therefore, we could conclude that biomineralization is indeed highly conserved and is mediated by a previously untargeted druggable pathway.

The production of calcium carbonate is associated with biofilm formation in CF sputum

Biofilm mineralization was not previously demonstrated in the lung microenvironment. To test the ability of lung pathogens to form structured communities in such conditions, we grew *M. abscessus* and *P. aeruginosa* on a synthetic CF sputum medium (SCFM). Both species were capable of forming highly organized 3D colonies on SCFM (Figure S12). Next, we examined whether calcite formation by lung pathogens could also be observed in clinical samples. We collected sputum samples from CF patients chronically infected with *P. aeruginosa* and removed the organic matter with bleach. Insoluble material indicating the presence of a mineral was found in 31 out of 50 samples examined (Table S1). These putatively positive patients were further analyzed by FTIR for residual pure minerals and spectra typical of calcite, lacking a $\nu 1$ peak and containing a ν_2 peak at 875 cm^{-1}, ν_3 peak at 1425 cm^{-1}, and ν_4 peak at 713 cm^{-1} (Figure S13), were identified in 7 samples.

The effect of calcium carbonate production on microbial colonization of an *Ex vivo* lung

To further explore the role of biomineralization during lung infection by *P. aeruginosa*, we set up a lung *ex vivo* model. Organ cultures derived from lung and colon tissues have been applied previously to study biofilm infections and viral tropism (Kolodkin-Gal et al., 2007, 2008; Massler et al., 2011; Wu et al., 2021) and thus can potentially be used to study lung infections. We cultured mice lungs and then infected them with *P. aeruginosa* constitutively expressing GFP. Fluorescent microscopy revealed biofilms forming on the tissue before its destruction (Figure S14). We then tested the effect of chemically blocking biomineralization during initial infection stages using this system. In the absence of *P. aeruginosa* inhibitors showed little or no toxicity to the tissue at measured concentrations (Figures S15). When left untreated, *P. aeruginosa* infected tissue (labeled by DAPI for visualization) has completely deteriorated. Infection in the presence of urease inhibitor AHA prevented biofilm formation and rescued the lung tissue (Figure 5A). Although the tissue was rescued, the bacterial load in the growth media remained similar (Figure 5B). This is consistent with the *in vitro* results presented above – as in all cases, inhibition of biomineralization prevented biofilm formation but had little effect on planktonic growth. This further strengthens our proposed hypothesis, suggesting biomineralization is a specific and controlled developmental feature of bacterial biofilms. To quantify the effects of urease inhibition during lung tissue infection, the tissue was stained with H&A, and the nuclei were counted (Figures 5C and 5D). We observed a significant rescue of the infected tissue by AHA in a dose-dependent manner. In agreement with these findings, the growth of bacteria in the medium was not reduced by AHA addition, but their colonization of the lung tissue was largely compromised (Figures 5E and 5F). Quantifying minerals confirmed the accumulation of bleach insoluble material in the lung following PA infection (Figure S16).

Significant reduction of lung cell death during infection by *P. aeruginosa* was also obtained with CA and calcium uptake inhibitors (Figures 6A–6C) and with mutants lacking CAs (Figure 6D). Consistent with our observation that both Diamox and AHA inhibited lung colonization and subsequent cell death, the combination of both was additive (Figure 6E). At the concentrations used here, AHA and DTNB were slightly toxic to the uninfected lung tissue, whereas SMV and Diamox had no adverse effect (Figure S14). Notably, calcium carbonate inhibitors were more efficient in halting complex pattern formation (Figure 3) compared with the inhibition of lung colonization (Figures 5 and 6). Still, the trends and the significance of inhibition were similar. We can therefore conclude that the entire biomineralization pathway, rather than a specific enzyme, is of crucial importance to host infection.

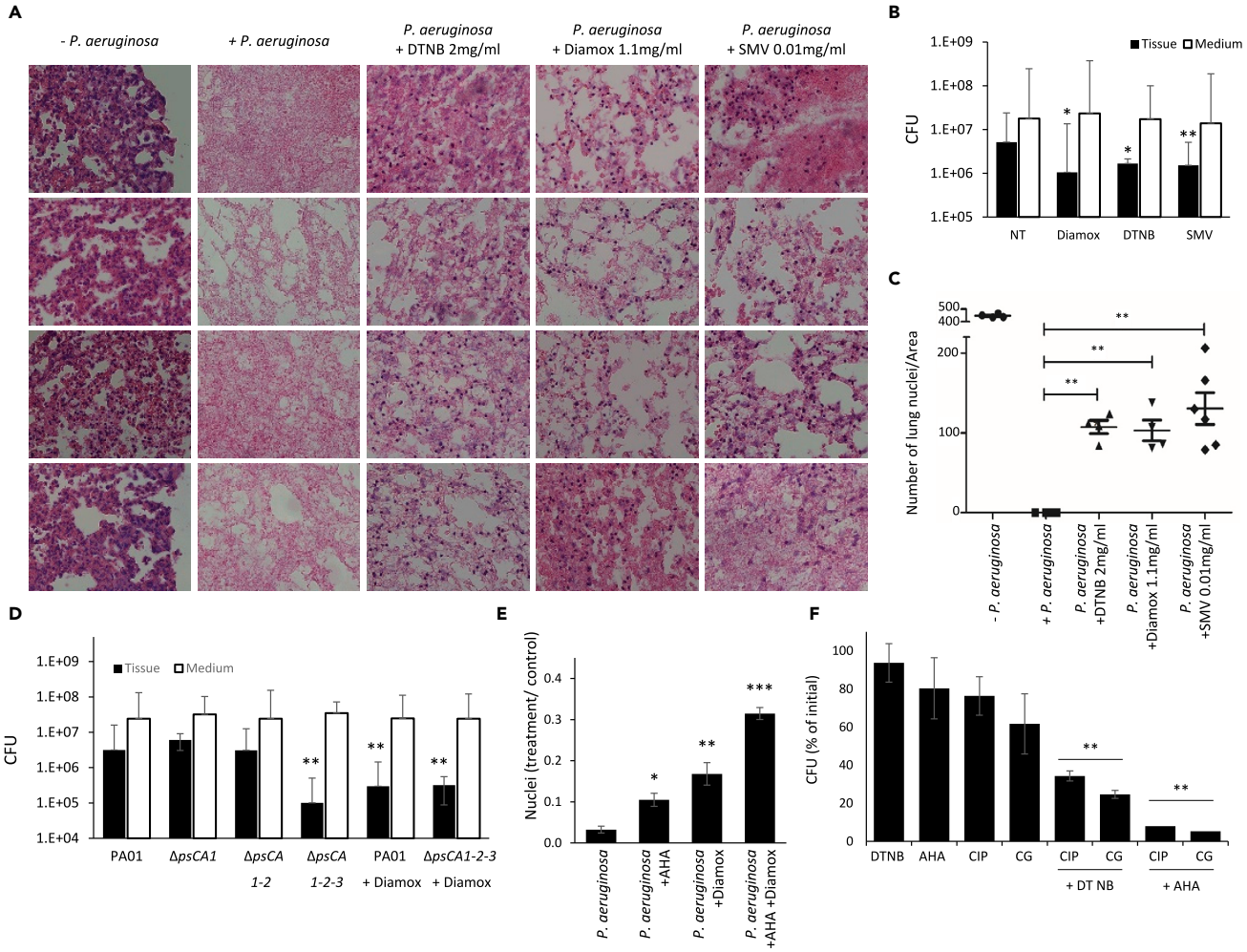

Figure 6. Inhibition of calcium carbonate production prevents biofilm formation and tissue deterioration in an *ex-vivo* lung model.

(A) Light microscopy images of 7 micron slices of lung tissues infected with *P. aeruginosa* PA14 and treated with biomineralization inhibitors as indicated. Samples were stained with H&E. Blue – nuclei, red – extracellular matrix and cytoplasm, (magnification ×40). A representative experiment (out of n = 3) experiments is shown.

(B) CFU of *P. aeruginosa* PA14 infecting lung tissue culture and surrounding media with and without indicated inhibitors (as in A). p values, as determined by Student's *t*-test are indicated (* pVal <0.01, ** pVal <0.001, when compared to the untreated control).

(C) Quantification of lung viability. Lung tissue cultures were infected with *P. aeruginosa* PA14 and treated with biomineralization inhibitors as indicated. ImageJ 1.51g software was used to automatically count lung cell nuclei in four randomly chosen fields for each treatment. p values, as determined by Student's *t*-test are indicated (** pVal <0.001).

(D) CFU analysis of wild type *P. aeruginosa* PA01 and the indicated mutants infecting lung tissue culture and surrounding media. Diamox was applied at 1.1 mg/mL, when indicated. p values, as determined by Student's *t*-test are indicated (* pVal <0.01, ** pVal <0.001, when compared to the untreated control).

(E) Quantification of lung viability. Lung tissue cultures were infected with *P. aeruginosa* PA14 and treated with biomineralization inhibitors, as indicated (Diamox and AHA applied at 1.1 mg/m). ImageJ 1.51g software was used to automatically count lung cell nuclei in four randomly chosen fields for each treatment. p values, as determined by Student's *t*-test are indicated (** pVal <0.001).

(F) *P. aeruginosa* PA14 biofilms were grown for 72 h on TB agar. The colonies were physically divided into equal parts, harvested, and half was treated for 2 h, as indicated. CIP – Ciprofloxacin, 3 mg/mL; GC – gentamycin, 10 mg/mL; AHA – 2.5 mg/mL; DTNB – 2 mg/mL. Viability is expressed as the ratio of CFU between the treated and the untreated parts of a colony. Results are averages and standard deviation of three independent experiments. p values, as determined by Student's *t*-test are indicated (** pVal <0.001).

Finally, although the ability to rescue host tissue by inhibition of biomineralization is encouraging, in clinical settings, the eradication of bacteria is essential. We, therefore, tested whether inhibition of mineralization during lung infection of *P. aeruginosa* could increase its sensitivity to antibiotics. Although neither biomineralization inhibitors nor quinolone antibiotics (a first-line antibiotic for treating *P. aeruginosa* infections) (Hewer, 2017) could effectively eradicate established biofilms, the combination of both classes of drugs

significantly increased the sensitivity of biofilms to treatment (Figure 6F), highlighting the potential clinical applications of biomineralization inhibition.

DISCUSSION

Regulated calcification was found to mediate complex 3D biofilm structure in three phyla – the *firmicutes* spore former *B. subtilis* (Keren-Paz et al., 2018) and here in the actinobacterium *M. abscessus* (Figure 4), and the proteobacteria *P. aeruginosa* (Figure 1). The conserved nature of cellular pathways promoting biomineralization allowed us to prevent biomineralization in phylogenetically distinct bacteria by chemically and genetically inhibiting carbonate accumulation and calcium uptake (Figures 2, 3 and 4). These results support the notion that mineralization in biofilms is a well-defined developmental process. Similar to the formation of exoskeletons within higher animals, the presence of structured mineral layer within a biofilm leads to the formation of a macrostructure serving specific functions and increasing the fitness of the microbial community.

In this work, we demonstrate that calcium uptake and functionally conserved pathways of carbonate production led to the formation of a mineral macro-structure. Numerous studies of *B. subtilis, P. aeruginosa,* and additional biofilm formers established that complex colony architecture is dependent on the organic extracellular matrix (Branda et al., 2005; Colvin et al., 2012; Jones and Wozniak, 2017; Kobayashi and Iwano, 2012; Romero et al., 2010; Vlamakis et al., 2013). Thus, it is frequently hypothesized that the presence of the organic ECM components is sufficient for bacterial biofilm morphogenesis. However, previously for *B. subtilis* (Keren-Paz et al., 2018; Oppenheimer-Shaanan et al., 2016) and here, in *P. aeruginosa,* we demonstrate that mutants in cellular processes leading to biomineralization are deficient in biofilm formation (Figure 3). Therefore, both organic ECM components and biogenic minerals are essential but not sufficient for the formation of complex structures.

Although, ,bacteria relied on calcium carbonate to generate functional scaffolds in our settings, other minerals may serve similar functions. For example, deposition of calcium phosphate crystals in *P. mirabilis, P. vulgaris* and *P. rettgeri* biofilms blocks catheters in infected patients (Broomfield et al., 2009; Mathur et al., 2006; Tan et al., 2018), and urease-dependent calcium phosphate mineralization was shown to increase *P. mirabilis* resistance to ciprofloxacin (Li et al., 2016c) and increase its survival in dual-species biofilms (Li et al., 2016b). Importantly, the physiological role of calcium phosphate deposits within these medical biofilms and whether dedicated cells facilitate this process remain to be determined.

Intriguingly, we could observe the presence of bacterially produced calcite minerals in the sputum of some CF patients infected with *P. aeruginosa*. This observation raises the possibility that lung pathogens can generate functional minerals within the host. Although biofilm colonies formed on top of biofilm-inducing agar are a convenient model system mimicking many of the environmental and physical conditions of the host, it lacks the host itself. Although several murine models are available for the study of CF (such as *Cftr−/−* knockout mice), they all fail to replicate the acute lung disease and chronic bacterial infections characteristic of CF patients (Semaniakou et al., 2018). *Ex vivo* organ cultures are an experimental system that recapitulates the three-dimensional structure of the tissue and includes several cell types and a variety of extracellular matrix components. On the other hand, organ culture is a controlled microenvironment lacking compounding factors that play a role in any infection, such as the efficiency of drug delivery and the immune system (Kolodkin-Gal et al., 2007).

Using chemical inhibitors and mutants, we demonstrated that biomineralization by *P. aeruginosa* was necessary for lung deterioration and that preventing it could rescue the infected tissue. The fact the free-living bacteria do not seem to be affected by inhibiting biomineralization and remain in the culture. In contrast, the tissue itself is rescued, highlights the importance of host attachment during infection. It is also possible that the restrictive properties of crystalline minerals on the diffusivity and viscoelasticity could themselves be harmful to the host tissue. High concentrations of calcium were measured previously in lungs of CF patients (Roomans, 1986), making mineralization highly feasible for resident bacteria. Moreover, consistent with the protective role of the mineral for the bacterial biofilm, chemical or genetic inhibition of mineralization restored the sensitivity of the *P. aeruginosa* to antibiotic treatment (Figures 5 and 6).

Here we provide collective evidence that biomineralization is highly conserved,. Thus, it is of enormous clinical significance because it can yield innovative classes of broad-spectrum drugs to combat emerging biofilm infections.

Limitations of the study

Although this study has demonstrated the role of calcium carbonate in biofilm formation and during lung colonization *Ex vivo*, we did not provide an *in vivo* model to demonstrate the formation of deletion mutants involved in calcium carbonate formation during chronic lung infection. Crystalline calcium carbonate was detected in human CF patients, but no clinical trial was performed on potential therapies. In addition, although genetic mutations had similar phenotypes to the chemical inhibition of carbonic anhydrase, urease and calcium uptake, chemical inhibitors can potentially have off-target effects. This could be overcome by repeating the experiments with clean genetic mutations in mice.

STAR★METHODS

Detailed methods are provided in the online version of this paper and include the following:

- KEY RESOURCES TABLE
- RESOURCE AVAILABILITY
  - Lead contact
  - Materials availability
  - Data and code availability
- EXPERIMENTAL MODEL AND SUBJECT DETAILS
  - Bacterial strains
  - Human samples
  - *Ex-vivo* mouse model
- METHOD DETAILS
  - Bacterial strains
  - Biofilm assays
  - Phase microscopy
  - Planktonic growth assays
  - Antibiotic sensitivity essays
  - Micro-CT X-ray analysis
  - FTIR spectrophotometer analysis
  - *Ex vivo* lung infection system
  - Pathology in an *Ex vivo* lung infection system
  - Bacterial load (CFU) in *Ex vivo* lung infection system
  - Thermogravimetric analysis (TGA)
  - Quality control for figure assembly
- QUANTIFICATION AND STATISTICAL ANALYSIS

SUPPLEMENTAL INFORMATION

Supplemental information can be found online at https://doi.org/10.1016/j.isci.2022.104234.

ACKNOWLEDGMENTS

The Kolodkin-Gal lab (Weizmann Institute of Science) was supported by the Israel Science Foundation grant number 119/16, Israel Foundation grant number JSPS 184.20, Kamin grant by Israel Chief Scientist no. 67459, Israel Ministry of Science, Technology & Space (grant no. 713454), Ministry of Health (grant no. 713645), Angel-Fiavovich fund for ecological research, Dr. Barry Sherman Institute for Medicinal Chemistry, Kekst Family Institute for Medical Genetics and by the Helen and Milton A. Kimmelman Center for Biomolecular Structure & Assembly. IKG is a recipient of Rowland and Sylvia Career Development Chair. The electron microscopy studies were partially supported by the Irving and Cherna Moskowitz Center for Nano and BioNano Imaging (Weizmann Institute of Science). We thank Prof. Ehud Banin and to Itzhak Zander (Bar-Ilan University) for helpful discussions, and for providing PA01 strains.

AUTHOR CONTRIBUTIONS

MCC, DKG, AKP, EK and IKG designed the study. IKG, DKG, AKP, SP, SK, VB, and RS designed and performed experiments. MP, DM, MS, and GZ contributed reagents and methods. HM participated in the analysis of the experiments detailed in Figure S16. EK and IKG mentored. IKG wrote the paper.

DECLARATION OF INTERESTS

The authors have submitted a patent titled "methods of disrupting a biofilm and/or preventing formation of same." Publication number: 20210015889.

Received: April 28, 2020
Revised: August 18, 2021
Accepted: April 7, 2022
Published: May 20, 2022

REFERENCES

Aguilar, C., Vlamakis, H., Losick, R., and Kolter, R. (2007). Thinking about Bacillus subtilis as a multicellular organism. Curr. Opin. Microbiol. *10*, 638–643.

Barabesi, C., Galizzi, A., Mastromei, G., Rossi, M., Tamburini, E., and Perito, B. (2007). Bacillus subtilis gene cluster involved in calcium carbonate biomineralization. J. Bacteriol. *189*, 228–235.

Branda, S.S., Vik, S., Friedman, L., and Kolter, R. (2005). Biofilms: the matrix revisited. Trends Microbiol. *13*, 20–26.

Broomfield, R.J., Morgan, S.D., Khan, A., and Stickler, D.J. (2009). Crystalline bacterial biofilm formation on urinary catheters by urease-producing urinary tract pathogens: a simple method of control. J. Med. Microbiol. *58*, 1367–1375.

Bryers, J.D. (2008). Medical biofilms. Biotechnol. Bioeng. *100*, 1–18.

Bucher, T., Keren-Paz, A., Hausser, J., Olender, T., Cytryn, E., and Kolodkin-Gal, I. (2019). An active beta-lactamase is a part of an orchestrated cell wall stress resistance network of Bacillus subtilis and related rhizosphere species. Environ. Microbiol. *21*, 1068–1085.

Caimmi, D., Martocq, N., Trioleyre, D., Guinet, C., Godreuil, S., Daniel, T., and Chiron, R. (2018). Positive effect of liposomal amikacin for inhalation on mycobacterium abcessus in cystic fibrosis patients. Open Forum Infect. Dis. *5*, ofy034.

Cohen-Cymberknoh, M., Gilead, N., Gartner, S., Rovira, S., Blau, H., Mussaffi, H., Rivlin, J., Gur, M., Shteinberg, M., Bentur, L., et al. (2016). Eradication failure of newly acquired Pseudomonas aeruginosa isolates in cystic fibrosis. J. Cyst. Fibros. *15*, 776–782.

Colvin, K.M., Gordon, V.D., Murakami, K., Borlee, B.R., Wozniak, D.J., Wong, G.C., and Parsek, M.R. (2011). The pel polysaccharide can serve a structural and protective role in the biofilm matrix of Pseudomonas aeruginosa. PLoS Pathog. *7*, e1001264.

Colvin, K.M., Irie, Y., Tart, C.S., Urbano, R., Whitney, J.C., Ryder, C., Howell, P.L., Wozniak, D.J., and Parsek, M.R. (2012). The Pel and Psl polysaccharides provide Pseudomonas aeruginosa structural redundancy within the biofilm matrix. Environ. Microbiol. *14*, 1913–1928.

Costerton, J.W., Stewart, P.S., and Greenberg, E.P. (1999). Bacterial biofilms: a common cause of persistent infections. Science *284*, 1318–1322.

Dietrich, L.E., Okegbe, C., Price-Whelan, A., Sakhtah, H., Hunter, R.C., and Newman, D.K. (2013). Bacterial community morphogenesis is intimately linked to the intracellular redox state. J. Bacteriol. *195*, 1371–1380.

Dietrich, L.E., Teal, T.K., Price-Whelan, A., and Newman, D.K. (2008). Redox-active antibiotics control gene expression and community behavior in divergent bacteria. Science *321*, 1203–1206.

El Mammeri, N., Hierrezuelo, J., Tolchard, J., Camara-Almiron, J., Caro-Astorga, J., Alvarez-Mena, A., Dutour, A., Berbon, M., Shenoy, J., Morvan, E., et al. (2019). Molecular architecture of bacterial amyloids in Bacillus biofilms. FASEB J. *33*, 12146–12163.

Friedman, L., and Kolter, R. (2004). Two genetic loci produce distinct carbohydrate-rich structural components of the Pseudomonas aeruginosa biofilm matrix. J. Bacteriol. *186*, 4457–4465.

Guragain, M., Lenaburg, D.L., Moore, F.S., Reutlinger, I., and Patrauchan, M.A. (2013). Calcium homeostasis in Pseudomonas aeruginosa requires multiple transporters and modulates swarming motility. Cell Calcium *54*, 350–361.

Halloum, I., Carrere-Kremer, S., Blaise, M., Viljoen, A., Bernut, A., Le Moigne, V., Vilcheze, C., Guerardel, Y., Lutfalla, G., Herrmann, J.L., et al. (2016). Deletion of a dehydratase important for intracellular growth and cording renders rough Mycobacterium abscessus avirulent. Proc. Natl. Acad. Sci. U S A *113*, E4228–E4237.

Harris, K.D., and Kolodkin-Gal, I. (2018). Applying the handicap principle to biofilms: condition-dependent signalling in Bacillus subtilis microbial communities. Environ. Microbiol. *21*, 531–540.

Hewer, S.C.L. (2017). Antibiotic strategies for eradicating Pseudomonas aeruginosa in people with cystic fibrosis. Cochrane Database Syst. Rev. CD004197.

Hill, D., Rose, B., Pajkos, A., Robinson, M., Bye, P., Bell, S., Elkins, M., Thompson, B., Macleod, C., Aaron, S.D., et al. (2005). Antibiotic susceptabilities of Pseudomonas aeruginosa isolates derived from patients with cystic fibrosis under aerobic, anaerobic, and biofilm conditions. J. Clin. Microbiol. *43*, 5085–5090.

Hufnagel, D.A., Price, J.E., Stephenson, R.E., Kelley, J., Benoit, M.F., and Chapman, M.R. (2018). Thiol starvation induces redox-mediated dysregulation of Escherichia coli biofilm components. J. Bacteriol. *200*, e00389–17.

Jacobs, H.M., O'Neal, L., Lopatto, E., Wozniak, D.J., Bjarnsholt, T., and Parsek, M.R. (2022). Mucoid pseudomonas aeruginosa can produce calcium-gelled biofilms independent of the matrix components Psl and CdrA. J. Bacteriol., e0056821.

Jansson, C., and Northen, T. (2010). Calcifying cyanobacteria–the potential of biomineralization for carbon capture and storage. Curr. Opin. Biotechnol. *21*, 365–371.

Jo, J., Cortez, K.L., Cornell, W.C., Price-Whelan, A., and Dietrich, L.E. (2017). An orphan cbb3-type cytochrome oxidase subunit supports Pseudomonas aeruginosa biofilm growth and virulence. Elife *6*, e30205.

Jones, C.J., and Wozniak, D.J. (2017). Psl produced by mucoid Pseudomonas aeruginosa contributes to the establishment of biofilms and immune evasion. mBio *8*, e00864–17.

Keren-Paz, A., Brumfeld, V., Oppenheimer-Shaanan, Y., and Kolodkin-Gal, I. (2018). Micro-CT X-ray imaging exposes structured diffusion barriers within biofilms. NPJ Biofilms Microbiomes *4*, 8.

Keren-Paz, A., and Kolodkin-Gal, I. (2020). A brick in the wall: discovering a novel mineral component of the biofilm extracellular matrix. N. Biotechnol. *56*, 9–15.

Kobayashi, K., and Iwano, M. (2012). BslA(YuaB) forms a hydrophobic layer on the surface of Bacillus subtilis biofilms. Mol. Microbiol. *85*, 51–66.

Kolodkin-Gal, D., Zamir, G., Edden, Y., Pikarsky, E., Pikarsky, A., Haim, H., Haviv, Y.S., and Panet, A. (2008). Herpes simplex virus type 1 preferentially targets human colon carcinoma: role of extracellular matrix. J. Virol. *82*, 999–1010.

Kolodkin-Gal, D., Zamir, G., Pikarski, E., Pikarski, A., Shimony, N., Wu, H., Haviv, Y.S., and Panet, A. (2007). A novel system to study adenovirus tropism to normal and malignant colon tissues. Virology *357*, 91–101.

Li, W.Y., Ni, W.W., Ye, Y.X., Fang, H.L., Pan, X.M., He, J.L., Zhou, T.L., Yi, J., Liu, S.S., Zhou, M., et al. (2020). N-monoarylacetothioureas as potent urease inhibitors: synthesis, SAR, and biological evaluation. J. Enzyme Inhib. Med. Chem. *35*, 404–413.

Li, X., Chopp, D.L., Russin, W.A., Brannon, P.T., Parsek, M.R., and Packman, A.I. (2015). Spatial patterns of carbonate biomineralization in biofilms. Appl. Environ. Microbiol. *81*, 7403–7410.

Li, X., Chopp, D.L., Russin, W.A., Brannon, P.T., Parsek, M.R., and Packman, A.I. (2016a). In situ biomineralization and particle deposition distinctively mediate biofilm susceptibility to chlorine. Appl. Environ. Microbiol. *82*, 2886–2892.

Li, X., Lu, N., Brady, H.R., and Packman, A.I. (2016b). Biomineralization strongly modulates the formation of Proteus mirabilis and Pseudomonas aeruginosa dual-species biofilms. FEMS Microbiol. Ecol. *92*, fiw189.

Li, X., Lu, N., Brady, H.R., and Packman, A.I. (2016c). Ureolytic biomineralization reduces Proteus mirabilis biofilm susceptibility to ciprofloxacin. Antimicrob. Agents Chemother. *60*, 2993–3000.

Lotlikar, S.R., Kayastha, B.B., Vullo, D., Khanam, S.S., Braga, R.E., Murray, A.B., McKenna, R., Supuran, C.T., and Patrauchan, M.A. (2019). Pseudomonas aeruginosa beta-carbonic anhydrase, psCA1, is required for calcium deposition and contributes to virulence. Cell Calcium *84*, 102080.

Massler, A., Kolodkin-Gal, D., Meir, K., Khalaileh, A., Falk, H., Izhar, U., Shufaro, Y., and Panet, A. (2011). Infant lungs are preferentially infected by adenovirus and herpes simplex virus type 1 vectors: role of the tissue mesenchymal cells. J. Gene Med. *13*, 101–113.

Mathur, S., Suller, M.T., Stickler, D.J., and Feneley, R.C. (2006). Factors affecting crystal precipitation from urine in individuals with long-term urinary catheters colonized with urease-positive bacterial species. Urol. Res. *34*, 173–177.

O'Toole, G.A. (2011). Microtiter dish biofilm formation assay. J. Vis.Exp. 2437.

Oppenheimer-Shaanan, Y., Sibony-Nevo, O., Bloom-Ackermann, Z., Suissa, R., Steinberg, N., Kartvelishvily, E., Brumfeld, V., and Kolodkin-Gal, I. (2016). Spatio-temporal assembly of functional mineral scaffolds within microbial biofilms. NPJ Biofilms Microbiomes *2*, 15031.

Palmer, K.L., Mashburn, L.M., Singh, P.K., and Whiteley, M. (2005). Cystic fibrosis sputum supports growth and cues key aspects of Pseudomonas aeruginosa physiology. J. Bacteriol. *187*, 5267–5277.

Park, S.M., Lu, C.D., and Abdelal, A.T. (1997). Cloning and characterization of argR, a gene that participates in regulation of arginine biosynthesis and catabolism in Pseudomonas aeruginosa PAO1. J. Bacteriol. *179*, 5300–5308.

Phoenix, V.R., and Konhauser, K.O. (2008). Benefits of bacterial biomineralization. Geobiology *6*, 303–308.

Politi, Y., Arad, T., Klein, E., Weiner, S., and Addadi, L. (2004). Sea urchin spine calcite forms via a transient amorphous calcium carbonate phase. Science *306*, 1161–1164.

Rani, S.A., Pitts, B., Beyenal, H., Veluchamy, R.A., Lewandowski, Z., Davison, W.M., Buckingham-Meyer, K., and Stewart, P.S. (2007). Spatial patterns of DNA replication, protein synthesis, and oxygen concentration within bacterial biofilms reveal diverse physiological states. J. Bacteriol. *189*, 4223–4233.

Richards, J.P., Cai, W.L., Zill, N.A., Zhang, W.J., and Ojha, A.K. (2019). Adaptation of Mycobacterium tuberculosis to biofilm growth is genetically linked to drug tolerance. Antimicrob. Agents Chemther. *63*, e01213–19.

Romero, D., Aguilar, C., Losick, R., and Kolter, R. (2010). Amyloid fibers provide structural integrity to Bacillus subtilis biofilms. Proc. Natl. Acad. Sci. U S A *107*, 2230–2234.

Roomans, G.M. (1986). Calcium and cystic fibrosis. Scan Electron Microsc. *1986*, 165–178.

Semaniakou, A., Croll, R.P., and Chappe, V. (2018). Animal models in the pathophysiology of cystic fibrosis. Front. Pharmacol. *9*, 1475.

Serra, D.O., Richter, A.M., Klauck, G., Mika, F., and Hengge, R. (2013). Microanatomy at cellular resolution and spatial order of physiological differentiation in a bacterial biofilm. mBio *4*, e00103–00113.

Steinberg, N., Keren-Paz, A., Hou, Q., Doron, S., Yanuka-Golub, K., Olender, T., Hadar, R., Rosenberg, G., Jain, R., Camara-Almiron, J., et al. (2020). The extracellular matrix protein TasA is a developmental cue that maintains a motile subpopulation within Bacillus subtilis biofilms. Sci. Signal. *13*, eaaw8905.

Steinberg, N., and Kolodkin-Gal, I. (2015). The matrix reloaded: probing the extracellular matrix synchronizes bacterial communities. J. Bacteriol. *197*, 2092–2103.

Stewart, P.S., and Franklin, M.J. (2008). Physiological heterogeneity in biofilms. Nat. Rev. Microbiol. *6*, 199–210.

Stickler, D., Morris, N., Moreno, M.C., and Sabbuba, N. (1998). Studies on the formation of crystalline bacterial biofilms on urethral catheters. Eur. J. Clin. Microbiol. Infect. Dis. *17*, 649–652.

Supuran, C.T. (2011). Bacterial carbonic anhydrases as drug targets: toward novel antibiotics? Front.Pharmacol. *2*, 34.

Tan, Y., Leonhard, M., Moser, D., Ma, S., and Schneider-Stickler, B. (2018). Inhibitory effect of probiotic lactobacilli supernatants on single and mixed non-albicans Candida species biofilm. Arch. Oral Biol. *85*, 40–45.

Vlamakis, H., Chai, Y., Beauregard, P., Losick, R., and Kolter, R. (2013). Sticking together: building a biofilm the Bacillus subtilis way. Nat. Rev. Microbiol. *11*, 157–168.

Wermser, C., and Lopez, D. (2018). Identification of Staphylococcus aureus genes involved in the formation of structured macrocolonies. Microbiology (Reading) *164*, 801–815.

Wu, B.C., Haney, E.F., Akhoundsadegh, N., Pletzer, D., Trimble, M.J., Adriaans, A.E., Nibbering, P.H., and Hancock, R.E.W. (2021). Human organoid biofilm model for assessing antibiofilm activity of novel agents. NPJ Biofilms Microbiomes *7*, 8.

Xu, K.D., Stewart, P.S., Xia, F., Huang, C.T., and McFeters, G.A. (1998). Spatial physiological heterogeneity in Pseudomonas aeruginosa biofilm is determined by oxygen availability. Appl. Environ. Microbiol. *64*, 4035–4039.

Yoon, S.S., and Hassett, D.J. (2004). Chronic Pseudomonas aeruginosa infection in cystic fibrosis airway disease: metabolic changes that unravel novel drug targets. Expert Rev. Anti Infect.Ther. *2*, 611–623.

STAR★METHODS

KEY RESOURCES TABLE

REAGENT or RESOURCE	SOURCE	IDENTIFIER
Chemicals, peptides, and recombinant proteins		
acetohydroxamic acid (AHA)	Sigma-Aldrich	Cat. #159034
5,5′-Dithiobis(2-nitrobenzoic acid) (DTNB)	Sigma-Aldrich	Cat. #D8130
acetazolamide (Diamox)	Sigma-Aldrich	Cat. #A6011
sodium metavanadate (SMV)	Sigma-Aldrich	Cat. #590088
Bacterial and virus strains		
Pseudomonas aeruginosa PA14	Lab collection	N/A
Pseudomonas aeruginosa PA14, Ppuc-GFP (carb)	A kind gift from E. Banin	N/A
Pseudomonas aeruginosa PA01	Lab collection	N/A
Pseudomonas aeruginosa PA01 Δ*psCA1*	M. Patrauchan	N/A
Pseudomonas aeruginosa PA01 Δ*psCA1-2*	M. Patrauchan	N/A
Pseudomonas aeruginosa PA01 Δ*psCA1-2-3*	M. Patrauchan	N/A
Pseudomonas aeruginosa PA01 Δ*calC*	This manuscript	N/A
Pseudomonas aeruginosa PA01 Δ*pel*Δ*psl*	A kind gift from E. Banin	N/A
Mycobacterium abscessus ATCC 19977	A kind gift from D. Barkan	ATCC 19977
Pseudomonas aeruginosa PA14 Δ*pel*	Lab collection	N/A
Software and algorithms		
ImageJ	Free Software	https://imagej.nih.gov/ij/

RESOURCE AVAILABILITY

Lead contact

Further information and requests for resources and reagents should be directed to and will be fulfilled by the Lead Contact, Ilana Kolodkin-Gal (ilana.kolodki@mail.huji.ac.il).

Materials availability

Bacterial strains generated in this study are available from the lead contact upon request.

Data and code availability

- All data reported in this paper, including microscope images, will be shared by the lead contact upon request.
- This paper does not report original code.
- Any additional information required to reanalyze the data reported in this paper is available from the lead contact upon request.

EXPERIMENTAL MODEL AND SUBJECT DETAILS

Bacterial strains

M. abscessus ATCC 19977 was maintained in standard lysogeny broth (LB) medium, at 37°C, unless indicated otherwise.

Pseudomonas aeruginosa PA14, PA01, and their derivate mutant strains were maintained in standard LB medium at 30°C, unless specified otherwise.

A list of strains used in this study can be found in Key resources table below.

Human samples

Sputum was collected from adult patients diagnosed with cystic fibrosis (CF), during routine visits to the Pulmonology Institute and CF Center, Carmel Medical Center, Haifa, Israel and Hadassah-Hebrew University Medical Center, Jerusalem, Israel. Specific patient information can be found in Table S1. All patients positive for calcite were carrying chronic *pseudomonas* infections. The samples were collected under Helskinki approval to Prof. Eitan Keren 0456-17-HMO, informed consent was obtained from all subjects.

Ex-vivo mouse model

Lungs were harvested from 2-3 BALB/C male mice (one month old). All mice were housed in SPF conditions. Animal work was carried out under ethical approval MD-16-15035-1.

METHOD DETAILS

Bacterial strains

Deletion of *calC* in *Pseudomonas aeruginosa* PA01 was kindly provided by the Patrauchan lab and CA mutants. The lack of polar effect was confirmed by complementation of *calC* from an ectopic chromosomal loci (Figure S17), *ΔcalC attB::calC*. PA14 and its polysaccharides mutant were originally reported by the Kolter lab (Friedman and Kolter, 2004).

Biofilm assays

M. abscessus biofilms were grown on B4 biofilm-promoting solid medium (0.4% yeast extract, 0.5% glucose, and 1.5% agar) supplemented with calcium acetate at 0.25% v/v. *P. aeruginosa* biofilms were grown on TB medium, as described previously (Dietrich et al., 2013) or on Brain Heart Infusion Broth (BHI, Sigma-Aldrich) supplemented with 1% agar. SCFM medium (50 mM MOPS [pH 7.2], 93 mM NH_4Cl, 43 mM NaCl, 3.7 mM KH_2PO_4, 1 mM $MgSO_4$, and 3.5 μM $FeSO_4 \cdot 7H_2O$, 20 mM glucose, 6.3 mM glucose, 13 mM succinate) was prepared as in (Palmer et al., 2005) and supplemented with 1.5% agar. Biofilm colonies were incubated at 30°C and 37°C (for *P. aeruginosa* and *M. abscessus* respectively), in a sealed box for enriched CO_2 environment achieved by using the candle jar method. Crystal-violet biofilm assay was carried out as previously described (O'Toole, 2011). Biofilms were washed with PBS, incubated with 100 μL of 0.25% crystal violet solution (Sigma-Aldrich, Cat #548-62-9). Crystal violet was removed and stained biofilms were washed twice in PBS. Intensity was determined by extraction of the crystal violet with 95% ethanol and measuring OD_{595} in a spectrophotometer. A well incubated with sterile growth media served as a control.

When indicated, the medium was supplemented with the following inhibitors purchased from Sigma-Aldrich: acetohydroxamic acid (AHA) (Cat. #159034); 5,5′-Dithiobis(2-nitrobenzoic acid) (DTNB) (Cat. #D8130); acetazolamide (Diamox) (Cat.#A6011) and sodium metavanadate (SMV) (Cat.#590088). The concentrations used are indicated in the text.

Phase microscopy

Biofilm colonies were observed using a Nikon D3 camera or a Stereo Discovery V20" microscope (Tochigi, Japan) with objectives Plan Apo S ×0.5 FWD 134 mm or Apo S × 1.0 FWD 60 mm (Zeiss, Goettingen, Germany) attached to Axiocam camera, as required. Data were captured using Axiovision suite software (Zeiss).

Planktonic growth assays

All strains were grown from a single colony isolated over lysogeny broth (LB) plates to a mid-logarithmic phase of growth (4hat 37°C with shaking). Cells were diluted 1:100 in 150 μL liquid B4 medium in 96-well microplate (Thermo Scientific). Cells were grown at 30°C for 20 h in a microplate reader (Synergy 2, BioTek), and the optical density at 600 nm (OD_{600}) was measured every 15 min. Three independent experiments were conducted, with three technical repeats per plate.

Antibiotic sensitivity essays

Colonies treated as described were split into two symmetric sections, which were resuspended in 1 mL PBS (Biological Industries). One section was left untreated whereas the other half was treated with indicated antibiotics. Samples were thoroughly vortexed (5 min). The samples were then mildly sonicated

(BRANSON digital sonifier, Model 250, Microtip, amplitude 30%, pulse 2 × 5s). In all cases, to determine the number of viable cells, samples were serially diluted in PBS, plated on LB plates, and colonies were counted after incubation at 30°C overnight. Experiments were performed with five technical repeats.

Micro-CT X-ray analysis

Images of indicated magnification were taken using a Zeiss micro XCT 400 instrument (Pleasanton, CA, USA). Tomography was carried out using a micro-focused source set at 20 kV and 100 μA. 1200 separate 2D images were taken with a pixel size of 0.87 mm over 1800, exposure time of 30 s. Image analysis was carried out with Avizo software (VSG, Hillsboro, OR, USA).

FTIR spectrophotometer analysis

Calcite was collected as described: agar samples were slightly bleached with 6% sodium hypochlorite for 1 min to remove organic matter, washed with Milli-Q water twice and dehydrated in acetone. Sputum was collected from patients and stored in 4°C degrees, until organic matter was removed as described above.

FTIR spectra of the bleached samples were acquired in KBr pellets by using a NICOLET iS5 spectrometer (Thermo Scientific, Pittsburgh, PA, USA). The samples were homogenized in an agate mortar and pestle with about 40 mg of KBr, and pressed into a 7 mm pellet using a manual hydraulic press (Specac, Orpington, UK). Infrared spectra were obtained at 4 cm^{-1} resolution for 32 scans.

The infrared calcite spectrum has three characteristic peaks, designated ν_2, ν_3, and ν_4. Calcium carbonate ν_3 peak is expected at 1425 cm^{-1} for calcite, 1490 cm^{-1} for vaterite and 1475 cm^{-1} for aragonite. The calcium carbonate ν_2 peak is expected at 875 cm^{-1} for calcite, 850 cm^{-1} for vaterite and 855 cm^{-1} for aragonite. Finally, the calcium carbonate ν_4 peak is expected at 713 cm^{-1} for calcite, 750 cm^{-1} for vaterite and 715 cm^{-1} for aragonite (Politi et al., 2004).

Ex vivo lung infection system

Animal work was carried out under ethical approval MD-16-15035-1. Lungs were harvested from 2 mice (one month old) and placed in Petri dishes containing DMEM 5% FCS. We divided the tissue into circular pieces 3 mm in diameter with a biopsy punch and transferred to a 24 well plate (4-5 explants/well) with 450 μL DMEM. DMEM was applied with carbenicillin 100 μg/mL (Sigma-Aldrich) and chemical inhibitors, as indicated. To each respective well, either 50 μL DMEM (control) or *P. aeruginosa* (pretreated with chemical inhibitors when indicated and diluted within DMEM to attain OD_{600} 0.4) was added – with three technical repeats for each condition. Plates were either fixated as below for microscopy or alternatively evaluated for microbial load.

Pathology in an *Ex vivo* lung infection system

The plates were incubated at 37°C for ~2 days (52 h), washed twice with PBS, fixed with PFA 4% for 10 min, and imbedded in either cryosection (OCT) compound or paraffin. Paraffin samples were cut into 7 micron slices and stained with H&E; whereas cryosections were cut into 10 micron slices and placed on superfrost plus slides.

Bacterial load (CFU) in *Ex vivo* lung infection system

For CFU of bacteria infecting *ex vivo* tissue culture was set as described above: individual punches or their growth media were collected, punches were resuspended in 1 mL PBS (Biological Industries), and free-living bacteria were pelleted and resuspended in PBS at the same volume. Samples were thoroughly vortexed (5 min). The samples were then mildly sonicated (BRANSON digital sonifier, Model 250, Microtip, amplitude 30%, pulse 2 × 5s). In all cases, to determine the number of viable cells, samples were serially diluted in PBS, plated on LB plates, and colonies were counted after incubation at 30°C overnight.

Thermogravimetric analysis (TGA)

% Mineral was calculated by the weight loss of infected lung punches with their respective control. Samples were dried in 50°C. The weight lost associated with the calcite relates to the temperature range 650–800°C.

Quality control for figure assembly

All figures and assembled graphs were scanned with Proofig (Proofiger LTD, IL).

QUANTIFICATION AND STATISTICAL ANALYSIS

All details of quantification methods, statistical analysis and significance calculations are discussed in each figure legend.

The intact colonies were visualized under X-ray, and the obtained 2D images were used to generate high-resolution 3D image (see Keren-Paz et al., 2018 for details). Rotation of 360° was taken around an axis perpendicular to the biofilm surface. Results are of a representative experiment out of three independent repeats.